LAWRENCE
LIVERMORE
NATIONAL
LABORATORY

UCRL-PROC-236318

Comparison between S/1 and R/1 tests and damage density vs. fluence (rho(phi)) results for unconditioned and sub-nanosecond laser-conditioned KD2PO4 crystals

J. J. Adams, J. Jarboe, M. Feit, R. Hackel

November 7, 2007

SPIE - Boulder Damage Symposium
Boulder, CO, United States
September 24, 2007 through September 26, 2007

Disclaimer

Comparison between S/1 and R/1 tests and damage density vs. fluence ($\rho(\phi)$) results for unconditioned and sub-nanosecond laser-conditioned KD_2PO_4 crystals

J. J. Adams*, J. A. Jarboe, M. D. Feit, R. P. Hackel

Lawrence Livermore National Laboratory
7000 East Avenue, L-592
Livermore, CA 94550

ABSTRACT

We present S/1 and R/1 test results on unconditioned and 355 nm (3ω), 500 ps laser conditioned DKDP. We find up to ~2.5X improvement in fluence in the S/1 performance after 3ω, 500 ps conditioning to 5 J/cm^2. For the first time, we observe a shift to higher fluences in the R/1 results for DKDP at 3ω, 7 ns due to 500 ps laser conditioning. The S/1 results are compared to $\rho(\phi)$ results previously measured on the same DKDP crystal [1]. A consistent behavior in fluence was found between the S/1 and $\rho(\phi)$ results for unconditioned and 500 ps conditioned DKDP. We were successful at using Poisson statistics to derive a connection between the S/1 and $\rho(\phi)$ results that could be tested with our data sets by trying to predict the shape of the $\rho(\phi)$ curve. The value for the power dependence on fluence of $\rho(\phi)$ derived from the S/1 data was ~11 ± 50%. The results presented and discussed here imply a strong correlation between the damage probability (S/1) test and $\rho(\phi)$. We find a consistent description of the two test types in terms of a power law $\rho(\phi)$ and that this basic shape held for all cases, i.e. the shape was invariant between unconditioned and conditioned results.

Keywords: DKDP, bulk damage, laser-conditioning, sub-nanosecond laser, damage density, damage probability

1. INTRODUCTION

Large aperture, multi-kilo-joule laser systems often depend on KDP and DKDP crystals for frequency conversion [2-3]. At sufficiently high fluence, these crystals can suffer from bulk and surface damage that can adversely affect the quality of the downstream beam. Laser conditioning can be used to eliminate or greatly reduce the initiation of bulk damage in DKDP optics in the fluence range of interest. A very useful quantity to judge the effectiveness of laser conditioning at preventing bulk damage is $\rho(\phi)$. Previous $\rho(\phi)$ studies have shown that 3ω, 500 ps laser conditioning is very effective at increasing the damage resistance of DKDP optics [1]. However, $\rho(\phi)$ measurements typically require a large area test beam (~1 cm^2) and are in general difficult to make.

S/1 and R/1 small diameter beam damage tests [4-6] are much easier to perform than $\rho(\phi)$ testing. However, S/1 and R/1 tests measure only damage probability vs. fluence which is very useful for making qualitative comparisons of the damage performance between different crystals or different conditioning protocols but do not allow direct calculation of the number of bulk damage sites initiated in the crystal for a given exposure fluence. In this paper, we present for the first time results from S/1 and R/1 damage testing on unconditioned and 500 ps laser conditioned DKDP. We then compare these results to damage density vs. fluence ($\rho(\phi)$) results previously measured on the same crystal with the idea of finding a useful connection between the two data sets. Note all the damage testing discussed in this paper was conducted at a wavelength of either 351 nm or 355 nm and both will be referred to as 3ω throughout.

* Correspondence: 925 422-4663, adams29@llnl.gov

2. EXPERIMENTS

2.1 S/1 and R/1 Bulk Damage Testing Basics

S/1 and R/1 damage tests have been discussed previously in the literature [4-6]. The goal in this section is to describe our specific experimental test setup, how the damage probabilities are determined, and simple interpretations of the test results. The term "S/1" refers to a bulk damage test where a single-fluence is tested on each site. Specifically in our case, 10 sites on the crystal are irradiated with 150 shots at a fixed fluence. The number of sites that damage out of 10 irradiated gives the damage probability. For instance if 2 out of 10 sites damage at a given fluence, the damage probability at that fluence is 20%. The fluence is then changed by ±15% with 10 sites tested at each new fluence until damage probabilities between 0% and 100% are measured. A schematic of our experimental S/1 test setup is shown in Figure 1. The determination of the occurrence of bulk damage in each site tested is based on scatter from the HeNe probe beam as detected by the CCD camera. Our S/1 experiment has a damage detection limit of ~one bulk damage site (pinpoint) per volume tested, in other words, a sensitivity of 1. The curve shown on the left in Figure 2 is an example of an S/1 damage probability curve. A typical fluence error bar in this fluence range of ±1 J/cm^2 is also shown.

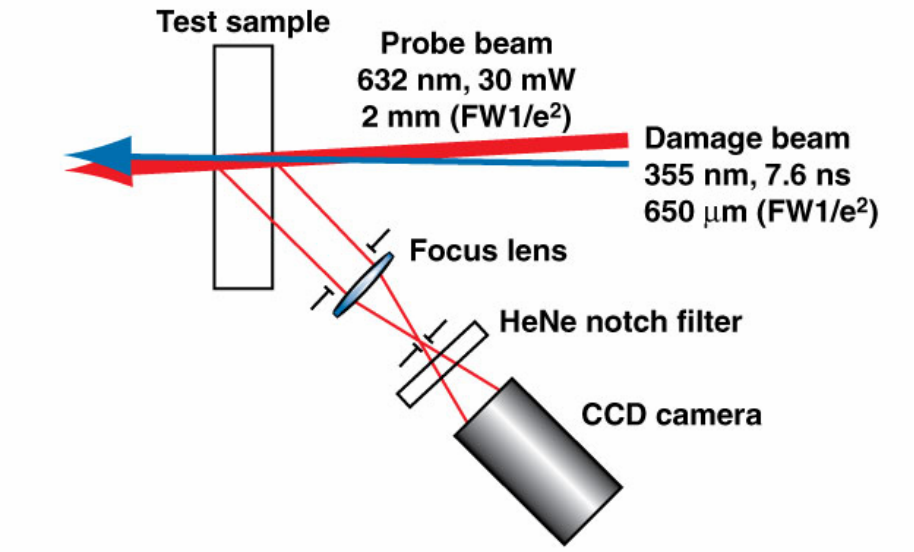

Figure 1: Schematic of the S/1 experimental test setup. The damage beam is produced by a pulsed, tripled Nd:YAG laser with an output wavelength of 355 nm (3ω). The laser has a Gaussian temporal profile with a pulse duration of 7.6 ns (referred to nominally as "7 ns" from here on) as labeled. The damage beam has a Gaussian spatial profile at the sample with full-width at 1/e^2 intensity of 650 μm and is collimated through the sample. The probe beam is produced by a CW HeNe laser with an output wavelength of 632 nm and output power of 30 mW. The probe beam has a Gaussian spatial profile at the sample with full-width at 1/e^2 intensity of 2 mm and is collimated through the sample. The probe beam is aligned to be collinear with the damage beam through the sample.

The term "R/1" refers to a bulk damage test where a ramped fluence is tested on each site. The schematic shown in Figure 1 is essentially our R/1 test setup with the only difference between what is shown and the R/1 setup is the CCD is replaced with a photomultiplier tube. Typically, 50-60 sites are individually irradiated with a ramped fluence until damage is detected. The determination of the occurrence of bulk damage in each site during the fluence ramp is based on scatter from the HeNe probe beam as detected by the photomultiplier tube. The fluence step between each shot in the ramp is 0.20 J/cm^2. The R/1 test setup has a bulk damage detection sensitivity of ~one bulk pinpoint per volume tested. For the case of exactly 50 sites tested, the R/1 damage probabilities are determined by assigning the highest fluence ramped to in the test a probability of 100%, the second highest fluence a probability of 98%, etc., with the lowest fluence

being assigned a probability of 2%. The curve shown on the right in Figure 2 is an example of an R/1 damage probability curve. A typical fluence error bar of ±10% is shown.

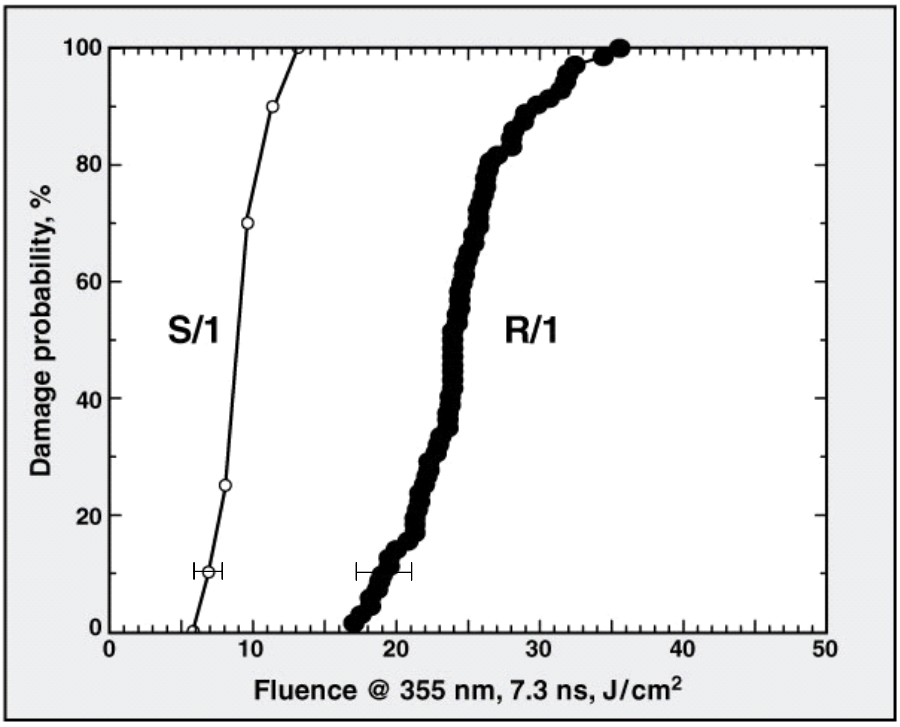

Figure 2: Example S/1 and R/1 damage test probabilities vs. 3ω, 7 ns test fluence. The lines connecting the data points in each curve are shown only as an aid to the eye. The errors bars shown represent a typical uncertainty in fluence for each test.

We interpret S/1 and R/1 damage test results in simple terms. Typically, the S/1 results are interpreted qualitatively as the damage performance that could be expected from unconditioned material (i.e. the "single-shot" unconditioned damage threshold). However, when S/1 testing is applied to previously conditioned material, it is interpreted as the "as prepared" or "conditioned" single-shot damage performance which can substantially differ from the unconditioned performance. The R/1 results are qualitatively interpreted as a measure of the best conditioning that could ever be achieved at the test wavelength and pulse length. In other words, the R/1 results can be interpreted as the "conditioned" damage performance. Note that neither of these two types of bulk damage tests directly measure bulk damage densities.

2.2 3ω, 500 ps Conditioning Laser

LLNL developed a 3ω, 500 ps laser system [7] to take advantage of the optimal conditioning pulse length range as discussed previously in [8]. The laser spot size at the conditioning plane was 1.2 mm in diameter. The diameter quoted is the diameter that encompasses 90% of the energy in the beam. A spatial profile for a typical pulse from the laser can be seen in Figure 3 a.). The beam's spatial profile is nominally a "top-hat" that can be approximated well by a 5^{th}-order super-gaussian. Unless otherwise stated, the fluences that will be reported will be the mean value for the fluence over the top 10% of the beam. The circular aperture seen in the figure is for reference and represents a diameter of 1 mm. The beam consistently has a 10% fluence contrast (standard deviation of the mean fluence/mean fluence). The laser operates at a pulse length of 500 ± 20 ps. A typical temporal pulse shape is shown in Figure 3 b.). Temporally, the pulse shape is also nominally "top-hat" and, as shown, has a FWHM of 520 ps that can be fit to a 2^{nd} order super-gaussian.

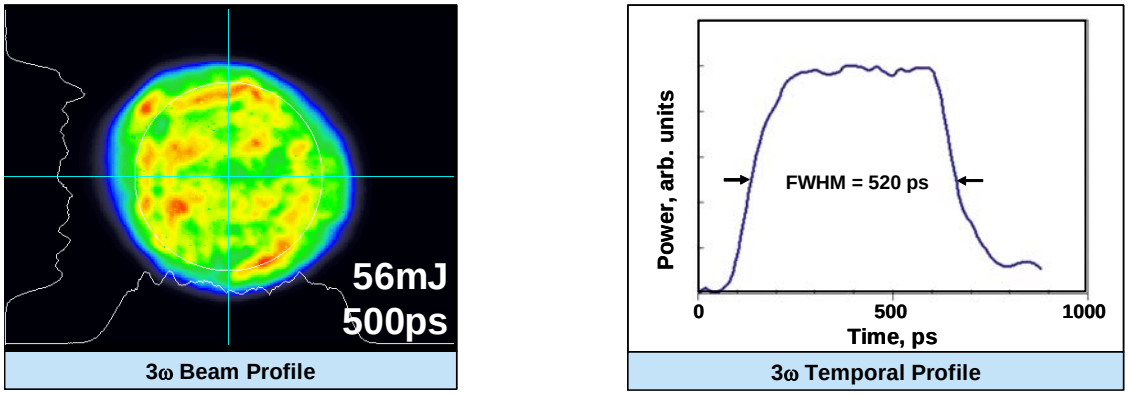

a.) b.)

Figure 3: a.) Spatial profile of the sub-nanosecond conditioning beam at the sample plane for a 56 mJ, 500 ps pulse as measured on a CCD. The line-outs at the bottom and left of the image are intensity line-outs spatially along the crosshairs. b.) Typical temporal profile for the sub-nanosecond conditioning laser as measured with the combination of a 45 GHz photo-detector and a sampling oscilloscope.

2.3 Scatter Map of the DKDP Sample

The sample used in the experiment was a 15 x 15 x 1-cm^3 plate fabricated out of conventional-growth DKDP and oriented for type II mixing of $1\omega + 2\omega \rightarrow 3\omega$. The surfaces of the sample were prepared with a diamond bit-turned finish and were uncoated. The sample was positioned during the experiments so that the direction of the 500 ps conditioning beam's polarization was aligned with the e-axis of the crystal and the input and output surfaces of the crystal during the damage testing were the same as for the conditioning scans.

Pristine regions on the sample were raster-scanned [4,9] with the 500 ps conditioning laser. The maximum conditioning fluences ramped to were 1, 3, 3.5, 4, 5 J/cm^2. An appropriate scan overlap and fluence step-size was used. The unconditioned and conditioned regions of the sample which were previously tested with single shots at 3 ns using a 0.9-cm beam [10] were subsequently S/1 and R/1 damage tested at 7 ns. Performing both types of damage tests on the same regions of a single sample greatly reduces any variation in the results due to sample-to-sample variability. The entire sample was photographed using a DMS set-up [10-11] which produced a 12-bit digital image of the sample. In a previous report [1] we discussed in detail the 3 ns damage testing of this sample, the results of which will be reviewed in section 3.3. Figure 4 shows a contrast-enhanced 12-bit electronic image [10-11] of the DKDP crystal after the conditioning scans, the single-shot damage testing at 3 ns, and the S/1 and R/1 damage testing at 7 ns. The arrays of sites tested in the S/1 and R/1 testing can be seen as labeled. The individual highly scattering sites appearing in the arrays, especially in the 1, 3.5, and 5 J/cm^2 conditioned regions is surface damage resulting from the S/1 and R/1 testing. The beam diameter used for the previous 3 ns testing was 9 mm as denoted in the figure. The clear aperture on the 15 cm part shown is 135 x 135 mm^2. The white boxes in Figure 4 denote the approximate regions ramp-conditioned with the 500 ps laser and the "to…" labels denote the maximum conditioning fluence used for each of the protocols. The numeric-only labels in the figure label selected 3ns test shot fluences. The testing that appears outside the white boxes (lower-left corner) are damage tests on the unconditioned region of the crystal. The regular horizontal white stripes along the right edge of the part are scatter from vacuum chuck marks [10]. The part shows a variety of small scatter sites over its surface primarily arising from surface particles and damage resulting from handling the crystal. Interestingly enough, as can be seen in the figure, for equivalent scatter intensity (damage density), the test fluences progressively get higher (i.e. 8 to 14 J/cm^2) as the conditioning fluence increases. The two very bright spots in the image at approximately the center and at the 8 o'clock position on the crystal is scatter from two large surface sites pre-existing on the crystal before any conditioning or testing.

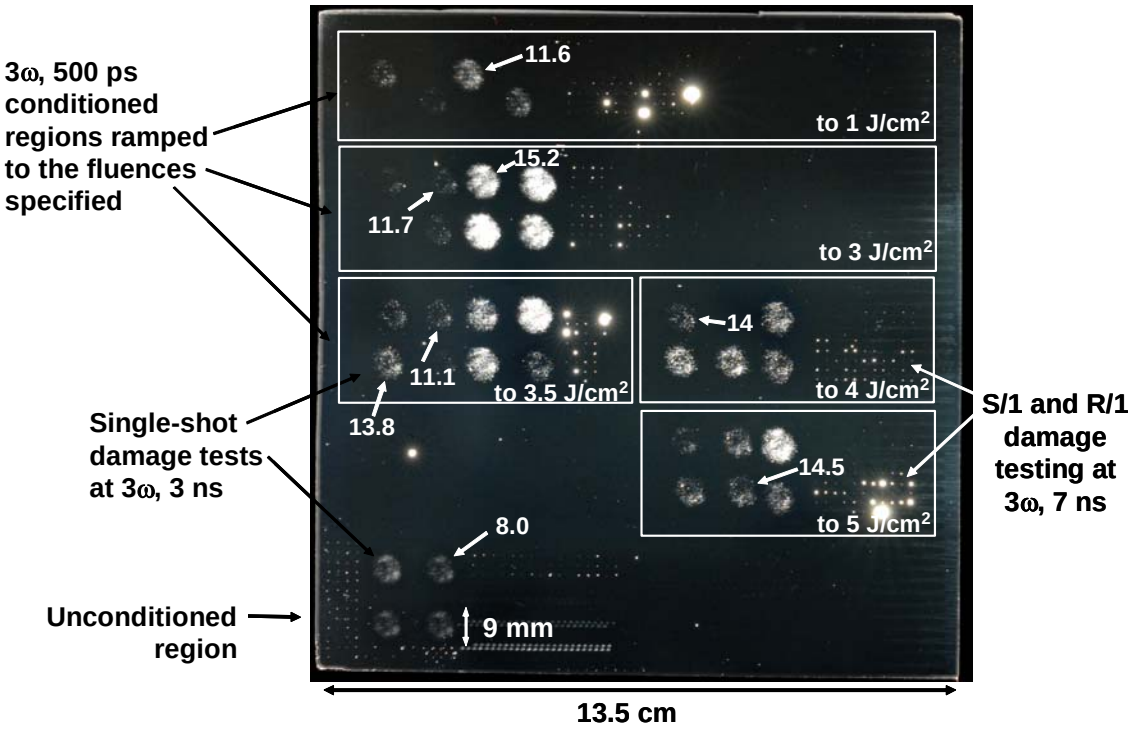

Figure 4: Contrast-enhanced 12-bit electronic image taken on a DMS [10-11] of the DKDP crystal after 3 ns single shot damage testing and S/1 and R/1 damage testing of the unconditioned and 500 ps conditioned regions. The white boxes denote the approximate regions ramp-conditioned with the 500 ps laser and the "to…" labels denote the maximum conditioning fluence used for each of the protocols. The arrays of scatter sites resulting from the S/1 and R/1 damage testing are as labeled. The white numeric-only labels in the figure label selected 3ns test shot fluences as discussed in [1]. Note, not all shots visible in the figure are labeled. The testing that appears outside the white boxes (lower-left corner) are damage tests (500 ps, 3 ns, 7 ns) on an unconditioned region of the crystal. The horizontal rows of evenly spaced scatter sites that appear in the unconditioned region directly above and below the "9 mm" label are bulk damage that resulted from single-shot damage tests at 500 ps and are not discussed in this report [1].

3. RESULTS AND DISCUSSION

3.1 S/1 and R/1 Bulk Damage Test Results for Unconditioned and 500 ps Laser-Conditioned DKDP

S/1 and R/1 damage testing was conducted on the unconditioned and 500 ps conditioned regions of the DKDP sample. Determining the S/1 and R/1 damage performance on the conditioned regions of the crystal allows us to qualitatively compare the effectiveness of increasing 500 ps conditioning fluence. Figure 5 shows a comparison of the results for the unconditioned and 500 ps conditioned to 5 J/cm^2 regions. The error bar for the unconditioned S/1 results represents a fluence uncertainty of ±1 J/cm^2 whereas the error bars on the unconditioned R/1 and the conditioned S/1 and R/1 represent ±10% fluence uncertainty. The lines connecting the data points in each curve are shown only as an aid to the eye. As can be seen, the S/1 and R/1 damage performance both show improvement to higher fluences after 500 ps laser conditioning to 5 J/cm^2. The S/1 and R/1 (50% probability point) results display ~2X and ~1.5X improvement in fluence, respectively, after the 500 ps conditioning to 5 J/cm^2. We choose to compare the R/1 data at the 50% points since in this range the experimental uncertainty is lowest as compared to the 0% and 100% ranges. In the past, we have conducted R/1 testing on >1 ns conditioned DKDP and have seen no shift between results on unconditioned and >1 ns conditioned DKDP as we see here. The shift in the R/1 curve after 500 ps conditioning is a new result and implies that a specific material modification has taken place after exposure to 3ω, 500 ps pulses that allow further conditioning of the sample at 3ω, 7 ns above and beyond its unconditioned state.

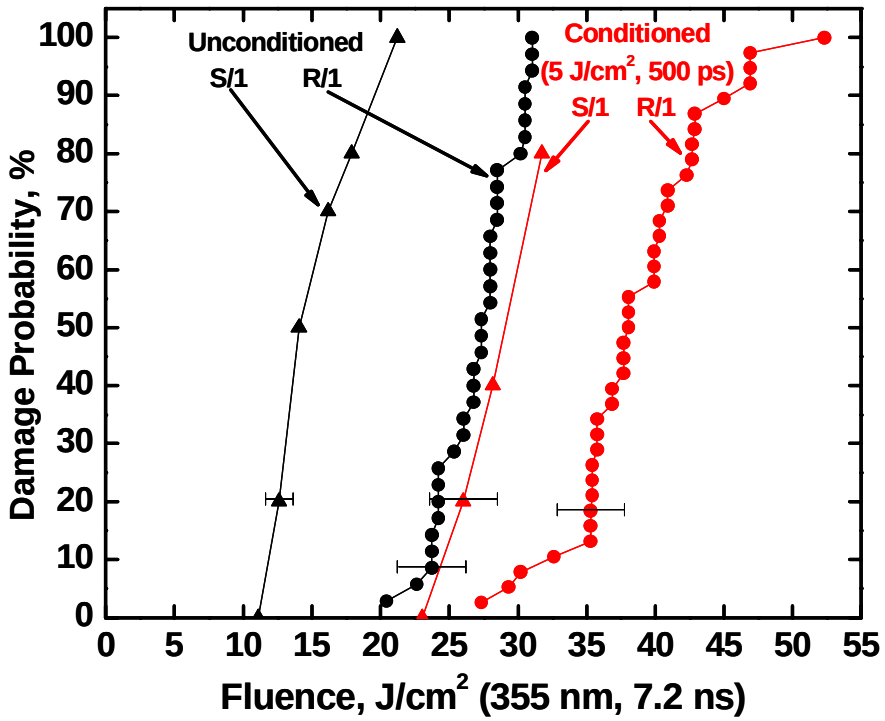

Figure 5: Plot of 3ω, 7 ns S/1 and R/1 damage test results for unconditioned and 500 ps conditioned (to 5 J/cm^2) DKDP. The error bar for the unconditioned S/1 results represents a fluence uncertainty of ±1 J/cm^2 whereas the error bars on the unconditioned R/1 and the conditioned S/1 and R/1 results represent ±10% fluence uncertainty. The lines connecting the data points in each curve are shown only as an aid to the eye. Note the ~2X improvement in fluence in the S/1 results after 500 ps laser conditioning to 5 J/cm^2 as well as the shift in the R/1 results to higher fluence.

Figure 6 shows a comparison between the S/1 and R/1 test results for the regions on the DKDP sample conditioned to 1, 3, 4, and 5 J/cm^2, 500ps. In both a.) and b.), the unconditioned results are shown for comparison and the labels denote the maximum conditioning fluence used in the different protocols. The lines connecting the data points in each curve are shown only as an aid to the eye. In Figure 6 a.), we see a systematic shift in the S/1 results to higher fluence for increasing conditioning fluence. Though some overlap between the error bar for the 3 J/cm^2 results and the 1 J/cm^2 and 4 and 5 J/cm^2 results can be seen, we believe the systematic shift to higher fluence of the 3 J/cm^2 results over the 1 J/cm^2 can still be interpreted as overall increase in the damage performance. However, there is no overlap between the error bars for the 1 J/cm^2 results and the 4 and 5 J/cm^2 results implying an unquestionable and distinct shift to higher fluence. This means the 4 and 5 J/cm^2 protocols were more effective than the 1 J/cm^2 protocol. As also can be seen, the S/1 results for the 4 and 5 J/cm^2 protocols are nearly identical in appearance and are certainly identical within the error bars. Therefore we conclude that the 500 ps conditioning effectiveness substantially decreases above 4 J/cm^2, or more generally, the S/1 results show a finite improvement in fluence with increasing 500 ps conditioning fluence. We will compare the S/1 results to previously measured $\rho(\phi)$ curves for these same regions on the crystal in section 3.3. We choose to compare the S/1 data to the $\rho(\phi)$ data as opposed to the R/1 data because, as stated earlier, the S/1 results can be interpreted as the "single-shot" damage threshold which is essentially what we probe when conducting the single-shot experiments to measure $\rho(\phi)$.

In Figure 6 b.), we see a systematic shift in the R/1 results to higher fluence for increasing conditioning fluence qualitatively very similar to the S/1 data. Depending on what probability value on the R/1 curves is chosen for comparison, i.e. 0% or 50% or 100%, the magnitude of the apparent shift changes. We are currently working to explain this observation. However in any case, if we take the 50% probability as our comparison point (which experimentally

makes sense since the uncertainty is highest in the 0% and 100% ranges and lower in the 50% range), the magnitude of the shift is not a much as for the S/1 test, i.e. ~1.5X vs. ~2X. We also see the same "saturation" in the improvement in the R/1 results with increasing conditioning fluence above 4 J/cm^2 as we did in the S/1 data. Overall, the S/1 and R/1 data sets have very similar qualitative behaviors with increasing 500 ps conditioning fluence.

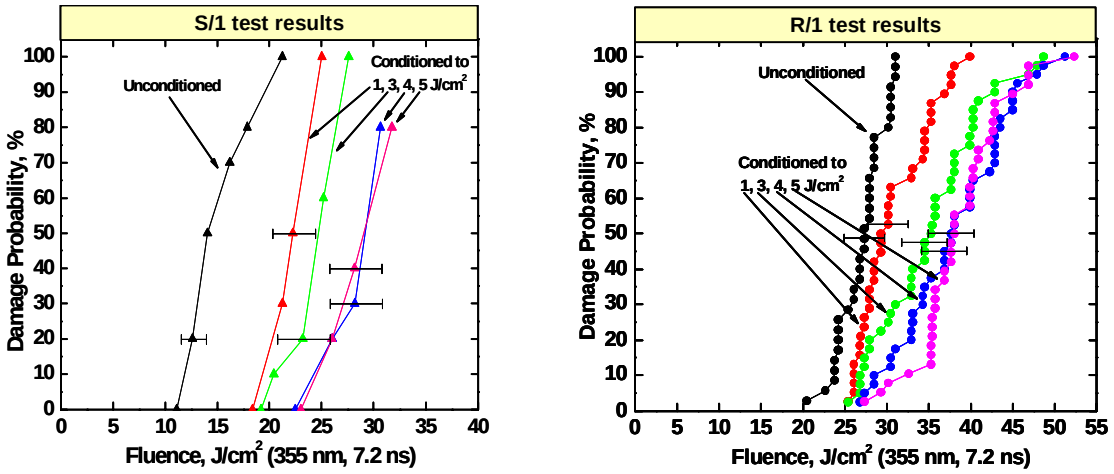

a.) b.)

Figure 6: a.) S/1 test results for the various 500 ps conditioning protocols. b.) R/1 test results for the various 500 ps conditioning protocols. In both cases, the unconditioned results are shown for comparison and the labels denote the maximum conditioning fluence used in the protocol for the region tested. The lines connecting the data points in each curve are shown only as an aid to the eye. Note the systematic shift to higher fluences in both sets of results.

3.2 Review of Technique to Measure Damage Density vs. Test Fluence, ρ(ϕ)

We review the technique used to determine the ρ(ϕ) curves discussed previously [8,12] for the unconditioned and 500 ps conditioned regions of our sample crystal. We have further discussed this technique in [1] and review it here only for completeness. Figure 7 illustrates the process in which ρ(ϕ) measurements are extracted from a damaged region on a crystal [12]. Basically, a single-shot is used to damage the crystal and then the number and spatial distribution of the bulk damage pinpoints are determined using an automated-scanning optical microscope. The microscope data is then combined with the fluence data to construct ρ(ϕ). The first step in the process is to damage a region on the crystal and record a calibrated image of the damaging beam's spatial profile from which the fluence distribution can be determined spatially over the beam. The next step is to use an automated-scanning microscope to size and position the pinpoints within the damaged bulk of the crystal. Since only a single color (3ω) was used for the damage testing, the distribution of the bulk damage along the beam propagation direction is uniform. Therefore only 3 mm of the 10 mm thickness of the crystal in each damaged region was scanned with the microscope. The automated microscope used for this study is a Summit 600 manufactured by VIEW Engineering, Inc. The pinpoint and fluence data is then averaged over 700 x 700 μm^2 bins. This size of bin was chosen out of convenience to speed up the data analysis without substantially impacting resolution. In the third step, the binned density and fluence data is independently ordered from low to high, and combined to construct an ordered-ρ(ϕ) curve which will be referred to as simply ρ(ϕ).

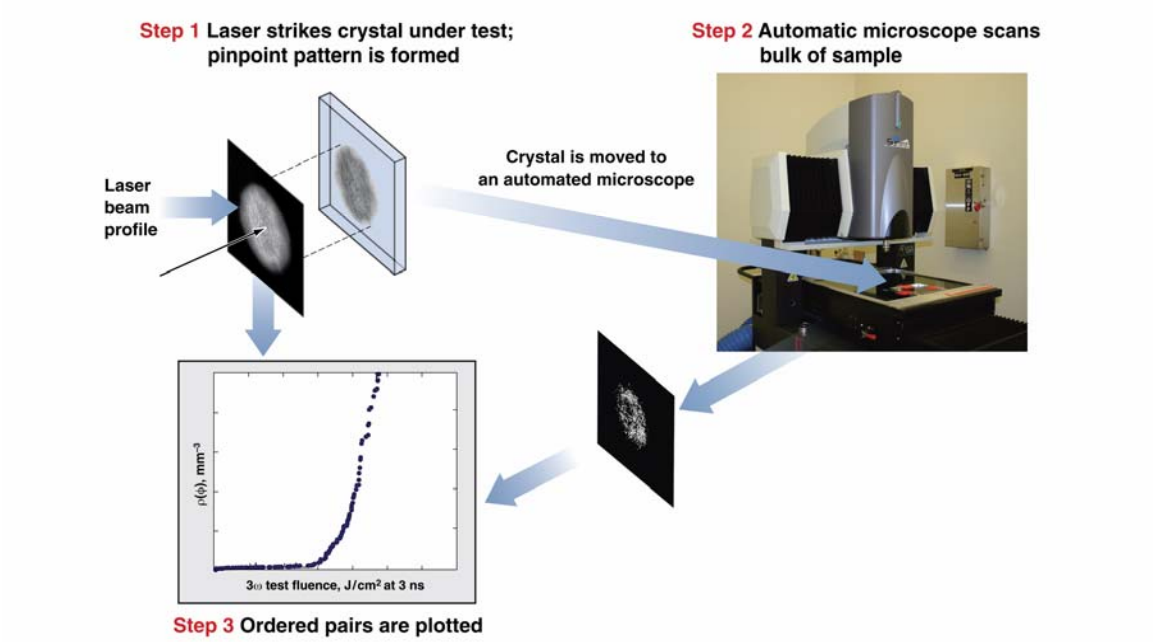

Figure 7: Process steps to extract ρ(ϕ) measurements from a laser-damaged region in a sample and the corresponding damaging beam's fluence spatial profile. The number and spatial distribution of the bulk damage pinpoints are determined using an automated-scanning optical microscope. The density and fluence data is binned, independently ordered from low to high, and combined [8,12] to construct the ρ(ϕ) curve.

It was determined that plotting the ρ(ϕ) data as ordered pairs (rather than x-y registered) produces a smooth well-behaved curve through the center of the noise in the x-y registered data [8]. In other words, the ordered plot of the data is very close to a numerical "best-fit" to the x-y registered data. The ordering is carried out by first sorting the binned fluence data from lowest to highest value independent of the pinpoint data and then sorting the binned pinpoint data similarly. Then the two sorted sets of data are put into one-to-one correspondence and plotted as shown in Figure 8 b.). For the current work, this technique may be considered the equivalent of ensemble smoothing the data (which yields similar results). We believe the ordered pairs plot is a sensible way to present the ρ(ϕ) data if the damage density is an increasing function of the fluence and the majority of the error sources are random. The contribution to the noise in the registered pairs plot has also been investigated by the authors and it has been concluded that it is very reasonable to use the ordered data for analysis. We point out that this type of testing and analysis is much more difficult and time consuming than S/1 and R/1 tests and so a method to predict ρ(ϕ) curves from S/1 or R/1 data would be very useful.

3.3 Comparison Between S/1 and ρ(ϕ) Results

Figure 8 shows a comparison between the results from the S/1 and ρ(ϕ) testing of the 500 ps conditioned regions on the crystal. In both a.) and b.), the unconditioned results are shown for comparison and the labels denote the maximum conditioning fluence used in the different protocols. In Figure 8 a.), the lines connecting the data points in each curve are shown only as an aid to the eye. The ρ(ϕ) data in Figure 8 b.) was originally presented and discussed in [1]. The lines through each of the data sets in Figure 8.b) are numerical fits of the form $a\phi^b$ where a and b are fitting parameters and ϕ is the fluence. Note the individual data sets in Figure 8 b.) are fairly well approximated by the fits (typical R^2 = 0.98). Examination of Figures 8 a.) and b.) reveal that the S/1 and ρ(ϕ) results have similar relative behaviors with conditioning. We can make several qualitative statements regarding the similarity of the S/1 and ρ(ϕ) results. First, both sets, including unconditioned and conditioned, are strong functions of the damaging fluence ($\phi^{\sim 8}$). Second, both results have approximately the same net shift in fluence (~2-2.5X) after 500 ps conditioning to 5 J/cm^2. Third, both show a finite improvement in fluence with increasing 500 ps conditioning fluence. These similarities in behavior with conditioning fluence between the S/1 and ρ(ϕ) results gives us further confirmation that we can qualitatively predict ρ(ϕ)

behavior from S/1 results. However, we would like a more quantitative relation between the two types of results with the ultimate goal of being able to accurately predict ρ(ϕ) curves from S/1 data.

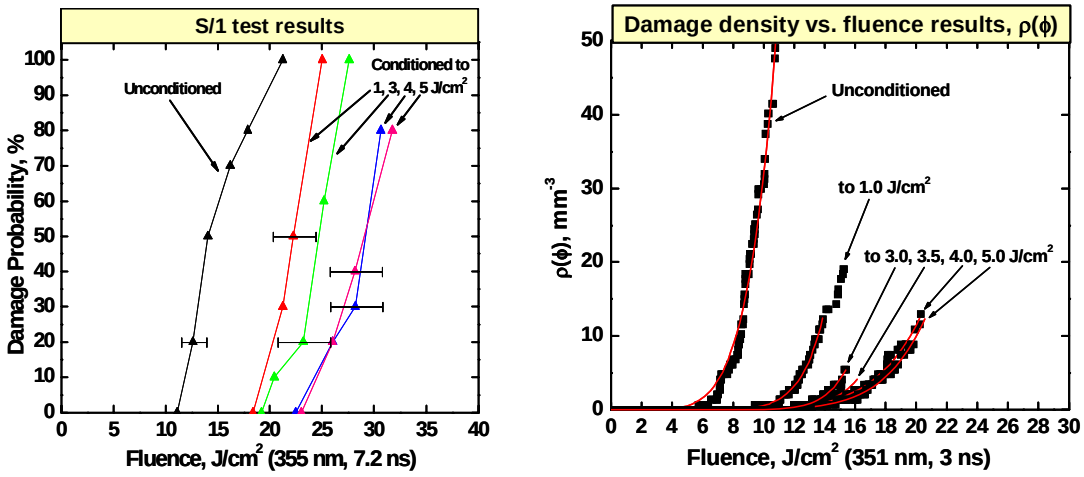

a.) b.)

Figure 8: a.) 3ω, 7 ns S/1 test results for the various 500 ps conditioning protocols. The lines connecting the data points in each curve are shown only as an aid to the eye. b.) Plot of ρ(ϕ) vs. 3ω, 3 ns test fluence for the different 500 ps conditioning protocols determined using the analysis discussed in section 3.2 [1,9]. The lines through each of the data sets in b.) are numerical fits of the form $a\phi^b$ where a and b are fitting parameters and ϕ is the fluence. Note an ~2.5X shift in fluence exists between the unconditioned ρ(ϕ) and the ρ(ϕ) corresponding to 500 ps conditioning to 5 J/cm^2. In both a.) and b.), the unconditioned results are shown for comparison and the labels denote the maximum conditioning fluence used in the protocol for each region tested. Also, note the test pulse length difference in the two sets of results, which does not affect the conclusions drawn in this section.

3.4 Brief Review of Poisson Statistics

Poisson statistics can be used to develop a straightforward connection between the S/1 and ρ(ϕ) results [13]. If we assume that in an area A, there exists a density of precursors, ρ, that are randomly distributed and the precursors are discrete and countable, then if we divide area A into n equal divisions, ΔA = A/n, we can write the probability, p, for finding a precursor in area ΔA as:

$$p = \rho \Delta A \tag{1}$$

Therefore the probability for <u>not</u> finding a precursor in area ΔA can be written as:

$$1-p = 1-\rho\Delta A \tag{2}$$

The probability for <u>not</u> finding a precursor in total area A, 1-P, can be written as:

$$1-P = (1-p)^n = (1-\rho\Delta A)^n = (1-\rho A/n)^n \rightarrow e^{-\rho A} \text{ as } n \rightarrow \infty \tag{3}$$

Therefore the probability function, P, for finding at least one precursor in total area A can be written as:

$$P = (1-e^{-\rho A}), \tag{4}$$

which we write for our case as:

$$P_{S/1}(\phi) = (1-e^{-\rho(\phi)V}), \tag{5}$$

where $P_{S/1}(\phi)$ is the S/1 probability as a function of fluence, $\rho(\phi)$ is the damage density vs. fluence, and V is the volume sampled. Keep in mind the above equation is an approximation which strictly speaking should contain the integral of $\rho(\phi)$ over the volume sampled. However, for small sample volumes and low precursor density (both of which apply to our case) the above is acceptable. As a test of the usefulness of the $P_{S/1}(\phi)$ expression, we will try to use it to predict the shape of the $\rho(\phi)$ curves from the S/1 data.

3.5 Estimating the Shape of the $\rho(\phi)$ Curve from the S/1 data

We will investigate estimating the shape of the $\rho(\phi)$ curve from the S/1 data using Eqn. (5). If we assume a power law dependence on fluence for $\rho(\phi)$ given by

$$\rho(\phi) = a\phi^b, \tag{6}$$

we can use the derived probability function (Eqn. (5)) to find a simple expression for b. If we take the ratio of Eqn. (5) evaluated at two probabilities, say 10% and 50%, we find the following expression for b:

$$b = \frac{\ln\left(\dfrac{\ln\left(\dfrac{1}{1-P_{50\%}}\right)}{\ln\left(\dfrac{1}{1-P_{10\%}}\right)}\right)}{\ln\left(\dfrac{\phi_{50\%}}{\phi_{10\%}}\right)} = \frac{1.8839}{\ln\left(\dfrac{\phi_{50\%}}{\phi_{10\%}}\right)} \tag{7}$$

We can now calculate b using Eqn. (7) and the measured S/1 fluences at probabilities of 10% ($P_{10\%} = 0.1$) and 50% ($P_{50\%} = 0.5$) from the data shown in Figure 8a.). The fluence values from Figure 8 a.) used for the calculation are shown in Table 1 (second and third columns). Note the fluence values found from Figure 8 a.), have been pulse length scaled [1,10,14] to an equivalent 3 ns pulse length using $\tau^{0.35}$. In the cases where an actual data point at the 10% or 50% probability value is not reported in Figure 8 a.), a 10% or 50% fluence value was found by averaging the fluence values of the two nearest probabilities that are reported. We show the calculated ratio of the 50% and 10% fluences ($\phi_{50\%}/\phi_{10\%}$) explicitly in Table 1 to point out the consistency in their values (1.19 ± 0.03) for the different cases. This is quite remarkable when one considers the potential sources of noise in the S/1 data such as energy and spot size fluctuations in the test laser, inhomogeneities in the crystal, and the fact that we are comparing unconditioned and conditioned results. This consistency strongly suggests that all the $\rho(\phi)$ curves have the same shape (aside from normalization). Note however, as shown in the parentheses in the $\phi_{50\%}/\phi_{10\%}$ column, each of the individual ratios has an uncertainty of ±20%.

The calculated values for b are shown in the "b from S/1 data" column of Table 1. As can be seen, the calculated values for b have a mean value of 10.8 with a standard deviation of ~±14%. However the individual values have much larger uncertainties on the order of ±50%. This is due to the sensitivity of the logarithm function to differences in decimal values around unity. Each value for the ratio $\phi_{50\%}/\phi_{10\%}$ has a ±20% uncertainty, as shown, and when this uncertainty is propagated through the logarithm function the result is a large (~±50%) uncertainty for the value calculated for b. Unfortunately this resulting large uncertainty hinders the accuracy of this method for determining the shape of the $\rho(\phi)$ curve. We will point out that our calculated values for b all agree within the error bars –albeit large error bars – and thus we conclude that we can only roughly estimate at this time the shape of the $\rho(\phi)$ curve using this method (i.e. only to within an uncertainty of ±50%). Other authors [15-16] have discussed in general a power-law dependence on fluence for $\rho(\phi)$ but we are the first to present numerical values for the power b.

For comparison, we also show values for the power b found from numerical fits to the $\rho(\phi)$ data in Figure 8 b.) as described in section 3.3. The errors quoted in the table are uncertainties to the least squares numeric fit of the data. As

can be seen, the values for b found from the fits are in general consistent and have a mean value of 7.5 ± 1.8 with the 10.5 value appearing to be the only significantly outlying data point (~1.5X deviation from the other values). This mean value agrees within errors to the values found from the analysis of the S/1 data. In fact, each of the values found from the fits agree within the error bars to the values found from the S/1 data since the error bars to those values are so large. However it is encouraging to note that the b values found both from the S/1 and $\rho(\phi)$ data agree within an order of magnitude implying that our analysis in either case is not grossly in error. We were successful at deriving a connection between the S/1 and $\rho(\phi)$ data that could be tested with our data sets and showed that S/1 results, like $\rho(\phi)$, are consistent with a power law dependence. We investigated the usefulness of the connection by trying to predict the shape of the $\rho(\phi)$ curve and found that uncertainties in our data significantly impacted our ability to predict the shape (power) of the $\rho(\phi)$ curve using this method.

Region	10% S/1 fluence ($\phi_{10\%}$)	50% S/1 fluence ($\phi_{50\%}$)	$\phi_{50\%}/\phi_{10\%}$ (± 20%)	b from S/1 data	b from $\rho(\phi)$ data
Unconditioned	**8.7**	**10.3**	**1.18**	**11 ± 6**	**6.0 ± 0.2**
to 1 J/cm^2	**14.2**	**16.4**	**1.15**	**13 ± 8**	**6.9 ± 0.2**
to 3 J/cm^2	**15.1**	**18.4**	**1.22**	**9 ± 5**	**10.5 ± 0.4**
to 4 J/cm^2	**17.9**	**21.6**	**1.21**	**10 ± 5**	**6.7 ± 0.2**
to 5 J/cm^2	**18.1**	**21.5**	**1.19**	**11 ± 6**	**7.6 ± 0.2**

Table 1: Calculated values for the $\rho(\phi)$ power dependence on fluence. The first column denotes the region of the crystal either unconditioned or conditioned at 500 ps to the stated maximum fluence. The second and third columns are pulse length scaled fluences at the 10% and 50% probability values obtained from the S/1 data shown in Figure 8 a.). The fourth column is the ratio of the fluence values from the second and third columns. The percentage shown in parentheses is the percent uncertainty to each of the ratios. The fifth column is the power value calculated using Eqn. (7) and the ratios shown in the fourth column. The last column shows power (parameter b) values found from a numerical fit of a power law to the $\rho(\phi)$ data shown in Figure 8 b) as discussed in section 3.3.

4. SUMMARY

The S/1 and R/1 bulk damage test procedures were described and a simple interpretation of the test results was discussed. The S/1 test is interpreted qualitatively as the unconditioned or "as prepared" single-shot damage threshold and the R/1 results can be interpreted as conditioned damage performance. Three types of damage testing (S/1, R/1, $\rho(\phi)$) were conducted on unconditioned and 500 ps conditioned regions of a single DKDP sample. The S/1 and R/1 damage results both show improvement in fluence after 500 ps laser conditioning. We see ~ 2X improvement in fluence in the S/1 results after 500 ps laser conditioning to 5 J/cm^2. The shift in the R/1 curves after 500 ps conditioning is a new result and implies that a specific material modification has taken place after exposure to 3ω, 500 ps pulses that allows further conditioning of the crystal at 3ω, 7 ns above and beyond its unconditioned state. A systematic shift in the S/1 and R/1 results to higher fluences for increasing 500 ps conditioning fluence is also observed. However, both the S/1 and R/1 results show only finite improvement with increasing conditioning fluence. Previously presented bulk damage density vs. fluence results ($\rho(\phi)$) [1] were reviewed. The $\rho(\phi)$ damage testing and analysis is much more difficult than S/1 and R/1 testing. Therefore, we compared results from the two test types to see if we could deduce $\rho(\phi)$ information from the S/1 results. Since the $\rho(\phi)$ results are based on single-shot damage tests it is most appropriate to compare $\rho(\phi)$ and S/1 results. Upon comparison, we find that the S/1 and $\rho(\phi)$ results have very similar relative behaviors with conditioning. Namely, both the S/1 and $\rho(\phi)$ results are strong functions of fluence, both have approximately the same net shift in fluence (~2-2.5X) after 500 ps conditioning to 5 J/cm^2, and both show a finite improvement in fluence with increasing 500 ps conditioning fluence. Poisson statistics were used to derive a straightforward quantitative connection between the S/1 and $\rho(\phi)$ results. We investigated the usefulness of the

connection by trying to predict the shape of the $\rho(\phi)$ curve. An expression relating the S/1 probability to $\rho(\phi)$ was derived and was used to find an expression that relates the power dependence on fluence for $\rho(\phi)$ to the S/1 data. Power values for the dependence on fluence of $\rho(\phi)$ were calculated from the S/1 data for unconditioned and 500 ps conditioned DKDP. The power values for the unconditioned and 500 ps conditioned cases in general agreed but only within large uncertainties (±50%), which means this is not the best method to determine the power. In general, we set out to connect $\rho(\phi)$ and S/1 and R/1 test results. The results presented and discussed here imply a strong correlation between the damage probability test and $\rho(\phi)$. We found a consistent description in terms of a power law $\rho(\phi)$ and that this basic shape held for all cases, i.e. the shape was invariant between unconditioned and conditioned results. We believe it is possible to more accurately predict the shape of $\rho(\phi)$ curves from S/1 and R/1 test results by using all the test results and not just that from two values of probability.

ACKNOWLEDGEMENTS

The authors wish to thank Clayton Dahlen for the artwork and Heather Platz and Paul Cattolica for cleaning and coating the crystals used in this work all with LLNL. This work performed under the auspices of the U.S. Department of Energy by Lawrence Livermore National Laboratory under Contract DE-AC52-07NA27344. UCRL-PROC-236318

REFERENCES

1. J. J. Adams, J. A. Jarboe, C. W. Carr, M. D. Feit, R. P. Hackel, J. M. Halpin, J. Honig, L. A. Lane, R. L. Luthi, J. E. Peterson, D. L. Ravizza, F. Ravizza, A. M. Rubenchik, W. D. Sell, J. L. Vickers, T. L. Weiland, T. J. Wennberg, D. A. Willard, M. F. Yeoman, "Results of sub-nanosecond laser-conditioning of KD_2PO_4 crystals," 2006 SPIE Proceedings, **6403**, 64031M-1 (2007)
2. J. J. De Yoreo, A. K. Burnham, P. K. Whitman, "Developing KH_2PO_4 and KD_2PO_4 crystals for the world's most powerful laser," Int. Mater. Rev. **47**, 113 (2002)
3. N. P. Zaitseva, J. Atherton, R. Rozca, L. Carmen, I. Smolsky, M. Runkel, R. Lyon, and L. James, J. of Crystal Growth **197**, 911 (1999)
4. M. Runkel and M. Nostrand, "An overview of raster scanning for ICF-class laser optics," 2002 SPIE Proceedings, **4932**, 136 (2003)
5. A. K. Burnham, M. Runkel, R. A. Hawley-Fedder, M. L. Carman, R. A. Torres, and P. K. Whitman, "Low-temperature growth of DKDP for improving laser-induced damage resistance at 350 nm," 2000 SPIE Proceedings, **4347**, 373 (2001)
6. R. Sharpe and M. Runkel, "Automated damage onset analysis techniques applied to KDP damage and the Zeus small area damage test facility," 1999 SPIE Proceedings, **3902**, 361 (2000)
7. J. Honig et al. to be submitted
8. J. J. Adams, T. L. Weiland, J. R. Stanley, W. D. Sell, R. L. Luthi, J. L. Vickers, C. W. Carr, M. D. Feit, A. M. Rubenchik, M. L. Spaeth, R. P. Hackel, "Pulse length dependence of laser conditioning and bulk damage in KD_2PO_4," 2004 SPIE Proceedings, **5647**, 265 (2005)
9. M. Runkel, K. Neeb, M. Staggs, J. Auerbach, A. K. Burnham, "The results of raster-scan laser conditioning studies on DKDP triplers using Nd:YAG and excimer lasers," 2001 SPIE Proceedings, **4679**, 368 (2002)
10. M. Runkel, J. Bruere, W. Sell, T. Weiland, D. Milam, D. Hahn, M. Nostrand, "Effects of pulse duration on bulk laser damage in 350-nm raster scanned DKDP," 2002 SPIE Proceedings, **4932**, 405 (2003)
11. F. Rainer, "Mapping and inspection of damage and artifacts in large-scale optics," 1996 SPIE Proceedings, **3244**, 272 (1997)
12. C. W. Carr, M. D. Feit, M. C. Nostrand, and J. J. Adams, "Techniques for qualitative and quantitative measurement of aspects of laser-induced damage important for laser beam propagation," Meas. Sci. Technol., **17**, 1 (2006)
13. M. D. Fiet, A. M. Rubenchik, M. R. Kozlowski, F. Y. Genin, S. Schwartz, L. M. Sheehan, "Extrapolation of damage test data to predict performance of large area NIF optics at 355 nm," 1998 SPIE Proceedings, 3578, 226 (1999)

14. M. Runkel, A. K. Burnham, D. Milam, W. Sell, M. D. Feit, A. M. Rubenchik, "The results of pulse-scaling experiments on rapid-growth DKDP triplers using the Optical Sciences Laser at 351 nm," 2000 SPIE Proceedings, **4347**, 359 (2001)
15. D. A. Cross, M. R. Braunstein, and C. W. Carr, "The effect of pulse duration on laser-induced damage by 1053-nm light in potassium dihydrogen phosphate crystals," 2006 SPIE Proceedings, **6403**, 64031U-1 (2007)
16. P. DeMange, C. W. Carr, H. B. Radousky, and S. G. Demos, "System for evaluation of laser-induced damage performance of optical materials for large aperture lasers," Rev. Sci. Instrum. **75**, 3298 (2004)